Available online at www.sciencedirect.com
SCIENCE DIRECT®
Sensors and Actuators B xxx (2006) xxx–xxx
SENSORS AND ACTUATORS B CHEMICAL
www.elsevier.com/locate/snb

Contrast enhancement of gas sensor array patterns with a neurodynamics model of the olfactory bulb

B. Raman, T. Yamanaka, R. Gutierrez-Osuna *

Department of Computer Science, Texas A&M University, College Station, TX, USA

Received 20 September 2005; accepted 5 January 2006

Abstract

We propose a biologically inspired signal processing model capable of enhancing the discrimination of multivariate patterns from gas sensor arrays. The model captures two functions in the early olfactory pathway: chemotopic convergence of sensory neurons onto the olfactory bulb, and center on–off surround lateral interactions. Sensor features are first topologically projected onto a two-dimensional lattice according to their selectivity profile, leading to odor-specific spatial patterning. The resulting patterns serve as inputs to a network of mitral cells with center on–off surround lateral inhibition, which enhances the initial contrast among odors and decouples odor identity from intensity. The model is validated using experimental data from an array of temperature-modulated metal-oxide sensors. Our results indicate that the model is able to improve the separability between odor patterns that is available at the inputs.

Keywords: Gas sensors; Electronic nose; Biologically inspired computation; Lateral inhibition; Contrast enhancement

1. Introduction

Pattern recognition for gas sensor arrays has traditionally relied on statistical or artificial neural network techniques [1–3]. Much can be learned, however, by studying the solutions that biological olfactory systems have developed over evolutionary time. Leveraging a growing body of knowledge from computational neuroscience [4], biologically inspired approaches to machine olfaction have become a recent subject of attention [5,6]. To the best of our knowledge, the earliest work on neuromorphic computation for gas sensor arrays was reported by Ratton et al. [7], who employed a model of olfactory bulb–cortex interactions developed by Ambros-Ingerson et al. [8] to classify data from micro-hotplate metal-oxide sensors. Kauer and co-workers [9,10] employed a spiking-neuron model of the peripheral olfactory system to process signals from a fiber-optic sensor array. Pearce et al. [11] investigated the issue of concentration hyperacuity by means of massive convergence of sensory inputs. Otto et al. [12] employed the KIII model of Freeman and co-workers [13] to process data from chemical sensors. Our group has previously developed computational models for odor mixture processing through habituation [14–16], gain control through shunting inhibition [17], and background suppression through cortical feedback [18].

This paper presents a detailed characterization of a contrast-enhancement model that incorporates two key principles in the early olfactory pathway: convergence of sensory inputs and lateral inhibitory circuits [19,20]. The model is validated on experimental data from an array of temperature-modulated metal-oxide semiconductor (MOS) chemoresistors. Our results are consistent with recent findings from neurobiology, and show that the model is able to enhance contrast between odor patterns beyond what is available in the raw inputs.

2. Neuromorphic model

Fig. 1 illustrates the basic structure of the proposed model. Signals from a chemosensor array are clustered onto a two-dimensional lattice so as to mimic the chemotopic convergence of olfactory receptor neurons (ORNs) inputs onto the olfactory bulb (OB). This initial "olfactory image" is then processed with a neurodynamics model that mimics the lateral inhibitory circuits in the bulb.

* Corresponding author. Fax: +1 979 847 8578.
E-mail addresses: barani@cs.tamu.edu (B. Raman), yamanaka@cs.tamu.edu (T. Yamanaka), rgutier@cs.tamu.edu (R. Gutierrez-Osuna).

0925-4005/$ – see front matter © 2006 Elsevier B.V. All rights reserved.
doi:10.1016/j.snb.2006.01.035

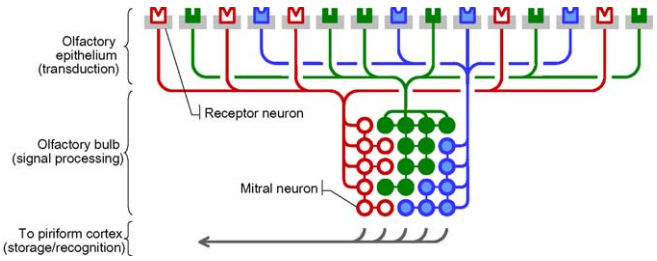

Fig. 1. Structure of the proposed model. Receptor neurons in the olfactory epithelium converge onto the olfactory bulb in a chemotopic manner, forming the first organized representation of a stimulus: an olfactory image. Contrast between the images for different odors is subsequently increased using center on–off surround lateral interactions in the olfactory bulb.

2.1. Input dimensionality

A fundamental difference between machine and biological olfaction is the dimensionality of the input space. The biological olfactory system employs a large population of ORNs (100 million neurons in the human olfactory epithelium, replicated from 1000 primary receptor types), whereas its artificial analogue uses very few sensors. The massively redundant representation used by the olfactory system improves signal-to-noise ratio, providing increased sensitivity in the subsequent processing layers [11].

To simulate a large population of cross-selective sensors we employ sensor modulation. In this approach, a suitable parameter that modifies the selectivity of the sensor must first be identified. In the case of MOS materials, the relative selectivity to different volatiles is known to be a function of the operating temperature at the surface of the material [21]. This operating temperature is typically maintained at a constant set-point (specified by the manufacturer) by applying a dc voltage across a resistive heater built into the device. This form of excitation is commonly referred to as isothermal operation. However, due to the abovementioned temperature-selectivity dependence of MOS devices, more information can be extracted from the sensor by simply modulating the heater voltage during exposure to a volatile and capturing the dynamic response of the sensor at each heater voltage. The process is illustrated in Fig. 2. We apply a sinusoidal voltage to the sensor's heater, and record the dynamic sensor response. If the heater voltage is modulated slowly enough relative to the thermal time constants of the device, the response of the sensor at each heater voltage can be considered a separate "pseudo-sensor", and used to simulate a large population of ORNs.

2.2. Chemotopic convergence

The projection from the olfactory epithelium onto the olfactory bulb is organized such that ORNs expressing the same receptor gene converge to one or a few glomeruli (GL) [22], globular structures of neuropil on which ORNs synapse mitral cells. This form of convergence serves two computational functions. First, massive summation of ORN inputs averages out uncorrelated noise, allowing the system to detect odorants below the detection threshold of individual ORNs [11]. Second, chemotopic organization leads to a more compact odorant representation than that available at the epithelium, providing the means to decouple odor quality from odor intensity. This is the basis for the traditional view of GL as labeled lines (one GL: one odor) or, more recently, as odotope detectors (one GL: one molecular feature) [23].

In ref. [24] we have presented a theoretical model of chemotopic convergence. The model is based on three principles: (i) ORNs with similar affinities project onto neighboring GL, (ii) GLs in OB are spatially arranged as a two-dimensional surface, and (iii) neighboring GL tend to respond to similar odors [25,26]. Therefore, a natural choice to model the ORN-GL convergence is the self-organizing map (SOM) of Kohonen [27].

In what follows, we will refer to pseudo-sensors as ORNs, and the SOM nodes to which the pseudo-sensors converge as GL. To form a chemotopic mapping, we must first define a selectivity measure upon which ORNs can be clustered together. In this work, this is accomplished by treating the ORN response across a set of odorants as an affinity vector:

$$\mathrm{ORN}_i = [\mathrm{ORN}_i^{\mathrm{O}_1}, \mathrm{ORN}_i^{\mathrm{O}_2}, \ldots, \mathrm{ORN}_i^{\mathrm{O}_C}] \quad (1)$$

where $\mathrm{ORN}_i^{\mathrm{O}_1}$ is the response of ORN_i to odor O, and C is the number of odorants.

The convergence model operates as follows. The SOM is presented with a population of ORNs, each represented by a vector in C-dimensional affinity space, and trained to model this distribution. Once the SOM is trained, each ORN is then assigned to

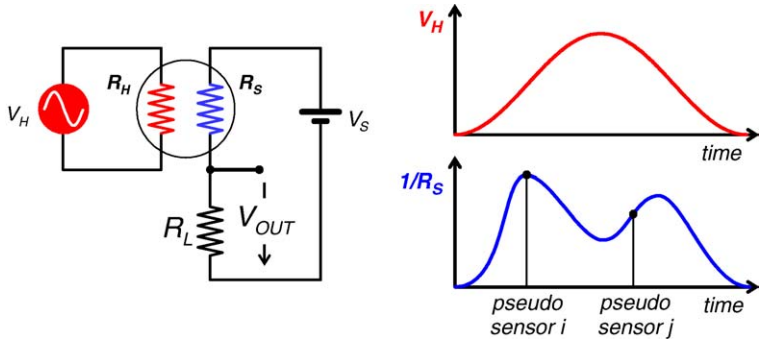

Fig. 2. Temperature modulation for metal-oxide sensors. A sinusoidal voltage V_H is applied to a resistive heater R_H, and the sensor resistance R_S is measured as a voltage drop across a load resistor R_L on a half-bridge. Due to the temperature-selectivity dependence, the response of a sensor at a particular temperature can be treated as a separate "pseudo-sensor," and used to simulate a large population of ORNs.

the closest GL in affinity space, thereby forming a convergence map from which the response of each GL is computed as:

$$G_j^{\mathrm{O}} = \sum_{i=1}^{N} W_{ij}\mathrm{ORN}_i^{\mathrm{O}} \tag{2}$$

where N is the number of ORNs in the array, and $W_{ij} = 1$ if ORN_i converges to GL_j and 0 otherwise.

This convergence model works well when the different sensors are reasonably uncorrelated, since then the projection of ORNs across the SOM lattice approximates a uniform distribution, i.e., maximum entropy [28]. Unfortunately, the population of pseudo-sensors created by temperature modulation is rather collinear. As a result, a few GL tend to receive the majority of ORNs, which capture the "common-mode" response of the sensor, overshadowing the most discriminatory information in the temperature-modulated response. To avoid this issue, the activity of each GL is normalized by the number of ORNs that converge to it:

$$G_j = \frac{\sum_{i=1}^{N} W_{ij}\mathrm{ORN}_i}{\sum_{i=1}^{N} W_{ij}}. \tag{3}$$

Note that this solution is not driven by biological plausibility but largely by the limitations of our sensors.

2.3. Center surround lateral inhibition

The initial glomerular image is further transformed in the OB by means of two distinct lateral inhibitory circuits. The first of these circuits, which occurs between mitral and inhibitory periglomerular (PG) cells, has been suggested to perform some form of "volume control" that broadens the dynamic range of concentrations at which an odorant can be identified [29]. The second circuit occurs through the interaction between mitral and inhibitory granule (G) cells at the output of the OB.

Two roles have been suggested for this granule-mediated circuit: (i) sharpening of the molecular tuning range of individual mitral cells [23], and (ii) global redistribution of activity such that the bulb-wide representation of an odorant, rather than the individual tuning ranges, becomes specific and concise over time [30]. More recently, both lateral circuits have been found to be center on–off surround inhibitory [31], an organization reminiscent of the classical receptive fields mediated by ganglion cells in the retina [32]. This form of lateral inhibition performs a winner-take-all competition, where strongly excited units suppress weakly excited ones. In the retina, center-surround leads to edge detection and discrimination of objects by size. In the context of olfaction, these circuits have been suggested to perform pattern normalization, noise reduction, and contrast enhancement of the spatial patterns in the OB [31].

We model this center on–off surround circuit with an additive model [33], whose general form is:

$$\frac{\mathrm{d}v_j(t)}{\mathrm{d}t} = -\frac{v_j(t)}{\tau_j} + \sum_{k=1}^{M} L_{kj}\varphi(v_k(t)) + I_j \tag{4}$$

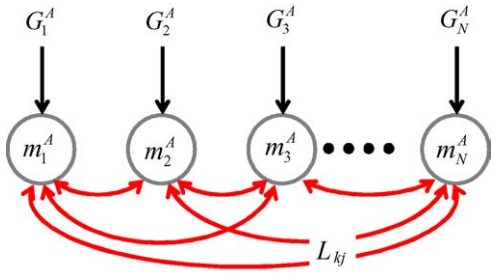

Fig. 3. Lateral inhibition at the output of the olfactory bulb.

where v_j is the activity of mitral neuron j, τ_j the time constant that captures the dynamics of the neuron, L_{kj} the synaptic weight between neurons k and j, M the number of neurons, and I_j is the external input in Eq. (3) properly scaled to balance the contribution of receptor and lateral inputs ($I_j = 10G_j$). Our model assumes a one-to-one mapping between GL and mitral neurons (refer to Fig. 3); although in some animal species GLs are known to project to several mitral neurons, the computational function of this divergence mapping is largely unknown. The non-linear activation $\varphi(\cdot)$ is the logistic function defined by:

$$\varphi(v_j) = \frac{1}{1 + \exp(-a_1(v_j - a_2))} \tag{5}$$

where the constants a_1 and a_2 are set to 0.0336 and 60.0335, respectively, to match the dynamic range of the signal. For simplicity, all mitral neurons are assumed to have the same time constant $\tau = 10$ ms.

Integration of Eq. (4) with Euler's method leads to a difference equation:

$$v_j(t + \Delta t) \cong v_j(t) + \Delta t\frac{\mathrm{d}v_j(t)}{\mathrm{d}t} = \left(1 - \frac{\Delta t}{\tau}\right) v_j(t) + \sum_{k=1}^{M} L_{kj}\varphi(v_k(t))\Delta t + I_j\Delta t \tag{6}$$

where the integration time step Δt was set to 1 ms for all the simulations presented in this paper.

To model center on–off surround, each neuron makes excitatory synapses to nearby units, and inhibitory synapses with distant units as follows:

$$L_{kj} = \begin{cases} U(a,b) & d(k,j) \le \dfrac{\sqrt{M}}{r} \\ U(-a,b) & \dfrac{\sqrt{M}}{r} < d(k,j) < \dfrac{2\sqrt{M}}{r} \\ 0 & d(k,j) \ge \dfrac{\sqrt{M}}{r} \end{cases} \tag{7}$$

where $U(a,b)$ is a uniform distribution between a and b, d the distance between units measured as a Euclidean distance within the lattice ($d = \sqrt{(\mathrm{row}_k - \mathrm{row}_j)^2 + (\mathrm{col}_k - \mathrm{col}_j)^2}$; row and col being the row and column coordinates of a neuron in the lattice), and r determines the receptive-field width of the lateral connections. Thus, the output of a given mitral neuron is determined by the combined effect of external inputs from ORNs, center on–off

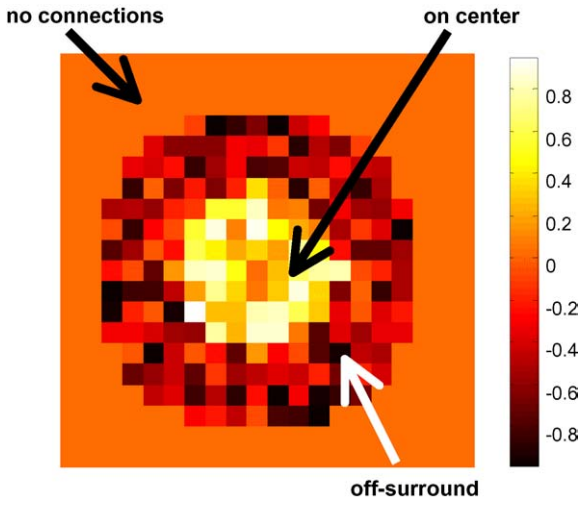

Fig. 4. An example center on–off surround receptive field in a 20×20 lattice for $r = 5$.

surround interactions with collateral neurons, as well as by its own dynamics. An example center on–off surround receptive field derived with Eq. (7) is shown in Fig. 4.

3. Experimental results

To validate the model, we have collected a database of temperature-modulated sensor patterns for three analytes acetone (A), isopropyl alcohol (B), and ammonia (C), at three different concentrations. Three replicas were sampled for each combination of analyte and concentration. Two Figaro MOS sensors (TGS 2600, TGS 2620) [34] were temperature modulated using a sinusoidal heater voltage (1–7 V; 2.5 min period; 10 Hz sampling frequency). The response of the two sensors (concatenated) to the three analytes at the three concentration levels is shown in Fig. 5a. Each point in the temperature cycle is considered as a separate pseudo-sensor, thus resulting in a population of 3000 pseudo-sensors. This population projects onto a GL layer with 400 nodes, arranged as a 20×20 SOM lattice, based on the convergence model described in Section 2.2. The SOM arranges itself to model the affinity space, as shown in Fig. 5b. Only one of the samples for the highest concentration of each odor was used to train the SOM; all the remaining samples and concentrations were used for validation purposes. The 400 outputs of the convergence model were used as the inputs to the neurodynamics OB model.

3.1. Spatial patterning

The temperature modulated patterns in Fig. 5a were processed with the proposed OB model. Fig. 6 (top row) shows the spatial pattern that results from sensory convergence at the input of the OB. As a result of the chemotopic mapping, each odor generates a unique spatial pattern across units in the SOM. However, these spatial patterns are highly overlapping due to the collinearity of the sensors. Fig. 6 (middle row) shows the resulting spatial activities following stabilization of the center-surround lateral interactions in Eq. (4). Odor A leads to heavy activation on two highly localized regions (spatial code: 13). Odor B produces similar activation in regions 1 and 3, but also high activation in region 4 (spatial code: 134). This unique region 4 corresponds to pseudo-sensors in the smaller peak that occurs for odor B alone (refer to Fig. 5a). Odor C produces heavy activation of regions 1, 2, and 5 (spatial code: 125). It is important to note that the location of these activation regions is concentration-invariant, but their amplitude and spread increases with concentration, in consistency with recent finding in neurobiology [35].

Fig. 6 only provides information about the steady-state response of the model. To analyze the temporal trajectory of each dynamic attractor, the 400-dimensional (20×20) space was projected onto the first three principal components of the data, as shown in Fig. 7. Trajectories for each odor and concentration originate at nearby locations in state space, which correspond to the highly overlapping spatial patterns at the input of OB, shown in Fig. 6 (top row). As a result of center on–off surround lateral connections, the activity for each odor slowly moves away from the initial location and settle into odor-specific fixed-point attractors, which correspond to the localized spatial patterns in Fig. 6 (middle row).

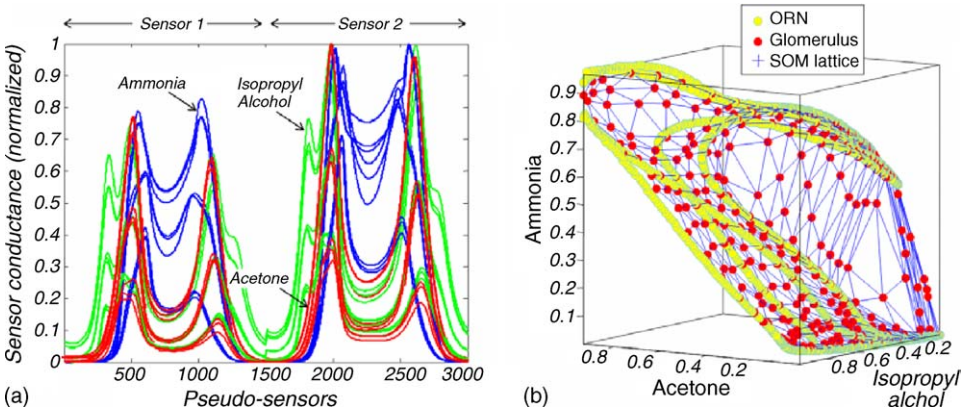

Fig. 5. (a) Temperature modulated response of two MOS sensors (concatenated) to acetone (odor A), isopropyl alcohol (odor B), and ammonia (odor C) at three concentrations. Three replicates per analyte and concentration are shown in the figure to illustrate the repeatability of the patterns. (b) Distribution of glomerular SOM nodes and pseudo-sensor repertoire in affinity space (3000 ORNs, 20×20 lattice).

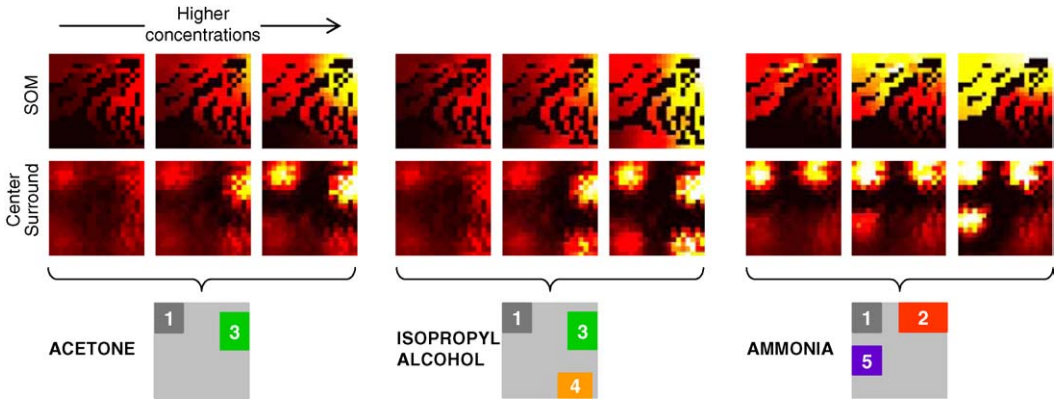

Fig. 6. Spatial maps at the input (top row) and output (middle row) of the olfactory-bulb network ($r = 5$). The bottom row shows the five sparse coding regions that emerge as a result of the lateral interactions.

Visual inspection of the steady-state response in Fig. 6 and the transient trajectories in Fig. 7 clearly show that the lateral inhibitory network is able to significantly increase the contrast between different odors. The separability of these patterns is analyzed systematically in the following section.

4. Analysis of results

4.1. Separability measure for odor patterns

To characterize the pattern-recognition performance of our model, we employ a measure of separability between categories related to the Fisher's discriminant analysis [36]:

$$J = \frac{\text{trace}(S_B)}{\text{trace}(S_W)} \tag{8}$$

where S_W and S_B are the within-class and between-class scatter matrices, respectively, defined as follows:

$$S_W = \sum_{q=1}^{Q} \sum_{x \in \omega_q} (x - \mu_q)(x - \mu_q)^T \tag{9}$$

$$S_B = \sum_{q=1}^{Q} (\mu_q - \mu)(\mu_q - \mu)^T \tag{10}$$

$$\mu_q = \frac{1}{n_q} \sum_{x \in \omega_q} x \quad \text{and} \quad \mu = \frac{1}{n} \sum_{\forall x} x \tag{11}$$

where x is a feature vector (in this paper, output or input pattern to the OB model), Q the number of odor classes, μ_q and n_q the mean vector and number of examples for odor q, respectively, n the total number of examples in the dataset, and μ is the mean vector of the entire distribution. Being the ratio of the spread between classes relative to the spread within each class, the measure J increases monotonically as classes become increasingly more separable.

Using this objective function, we introduce a novel measure that provides a tradeoff between concentration-invariant separability across odors and concentration separability within each odor. This measure favors representations where the odors are clustered hierarchically based first on their identity (main cluster) followed by their concentration levels (sub-cluster), as shown in Fig. 8.

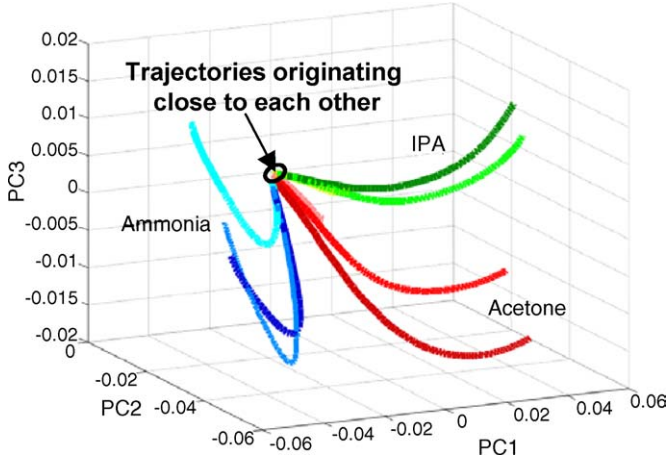

Fig. 7. Evolution of OB activity along the first three principal components of the data. Nine trajectories are shown, one per odor and concentrations in the data. The initial points in the trajectories are the spatial maps at the input of the OB network. Odor separability is improved as a result of lateral inhibition.

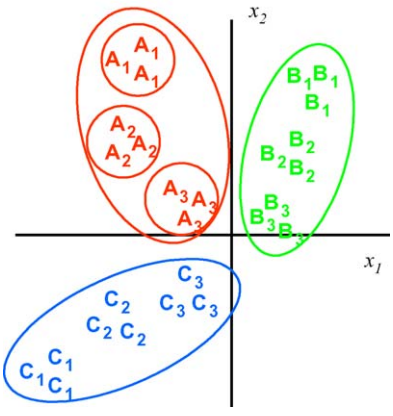

Fig. 8. Illustration of the separability measure J_{balance}. An ideal representation favored by the measure shows primary clusters corresponding to the odor identities (A–C), and sub-cluster within each odor cluster corresponding to each concentration level (A_3 indicating the last and lowest concentration for odor A).

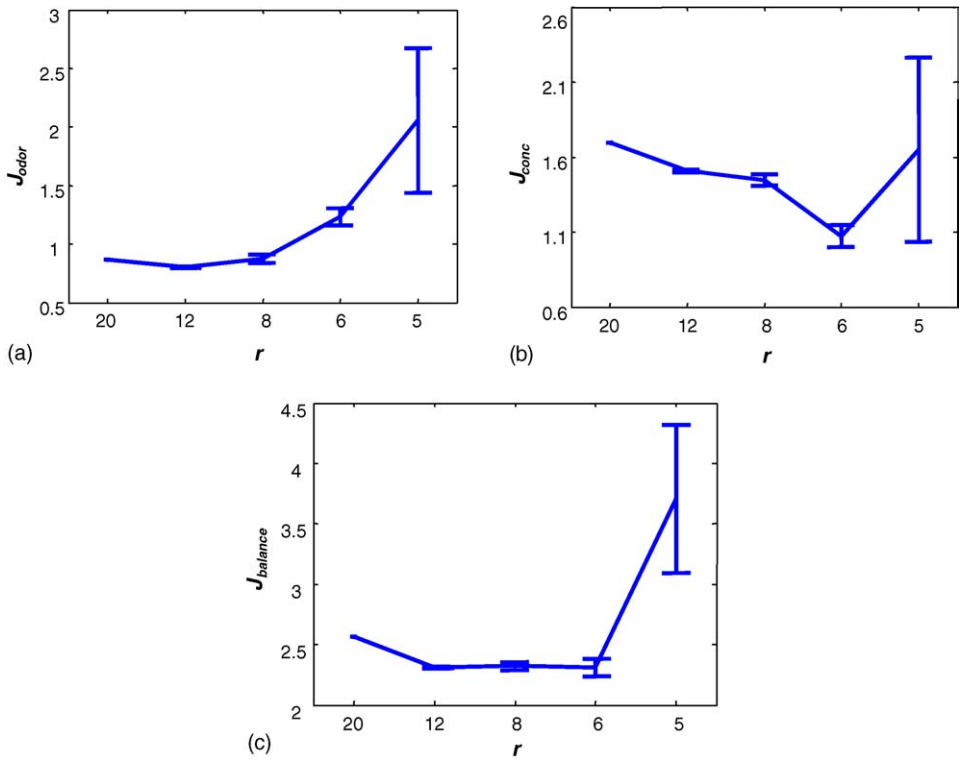

Fig. 9. Discriminatory information of GL patterns as a function of receptive field width: (a) separability between odors J_{odor}, (b) separability between concentrations within an odor J_{conc}, and (c) separability across odors and across concentrations.

The concentration-invariant separability is measured by:

$$J_{odor} = w_1 J_{AB} + w_2 J_{BC} + w_3 J_{CA} \quad (12)$$

where J_{AB}, J_{BC}, and J_{CA} are the separability between odors A and B, B and C, and C and A, respectively, and w_1, w_2, and w_3 are the normalization weights to prevent any pair of odors from dominating the metric.

The concentration separability within each odor class is defined by:

$$J_{conc} = w_4 J_{a1a2a3} + w_5 J_{b1b2b3} + w_6 J_{c1c2c3} \quad (13)$$

where J_{a1a2a3}, J_{b1b2b3}, and J_{c1c2c3} are the separability among the three concentrations within an odor, and w_4, w_5, and w_6 are normalization weights to balance the relative contribution of these three terms.

Contributions from these two measures are then added to yield a metric that balances odor-discrimination and concentration sensitivity:

$$J_{balance} = J_{odor} + J_{conc} \quad (14)$$

A suitable balance between these two terms can be found through the normalization weights w_1–w_6. In this paper, the normalization weights are set as the inverse of the maximum possible value of the corresponding term across all values of r, the width of lateral connections (e.g., $w_1 = 1/\max_{\forall r}(J_{AB})$). This scales each term J_{AB}, J_{BC}, J_{CA}, J_{a1a2a3}, J_{b1b2b3}, and J_{c1c2c3} between 0 and 1 making their contribution to J_{odor} and J_{conc} comparable.

4.2. Effect of receptive field width for the center surround connections

The width of the center on–off surround connections is an important parameter for the purpose of pattern formation and generalization. An appropriate value for receptive field width must provide both stability and good separability. Though the exact optimal value may depend on the database used, the general characteristics described below hold across various databases.

Fig. 9a–c shows the measures of concentration-invariant recognition (J_{odor}), concentration separability (J_{conc}), and their combination $J_{balance}$ ($J_{balance} = J_{odor} + J_{conc}$) as a function of the receptive field widths. Small receptive fields ($r > 4$) are primarily driven by inputs and hence show high stability (converge to a fixed-point attractor) and less variance. For large receptive fields ($r \leq 4$), the net value of the lateral connections becomes excitatory, and the system fails to converge into fixed-point attractors. Hence we will not consider them for determining the optimal parameter value for this odor database.

Fig. 9a and b shows the separability between various odors (J_{odor}) and across different concentrations within each odor (J_{conc}) as a function of the receptive field width (r). From these results, it is clear that that the separability between pairs of odors

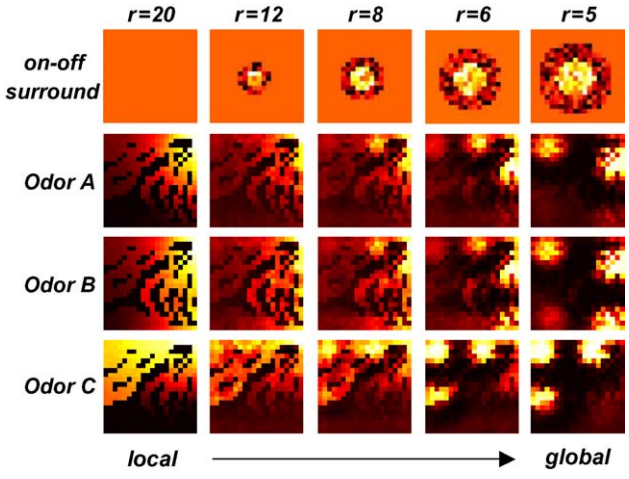

Fig. 10. Characteristics of the spatial odor code for various receptive-field widths of center on–off surround lateral connections. Global connections result in more sparse patterns that provide better odor separability.

increases as the width of the receptive field increases, whereas maximum concentration separability is achieved with small receptive fields. The maximum of the objective function J_{balance}, which combines concentration-invariant separability and concentration separability, occurs at $r = 5$, as shown in Fig. 9c. This receptive field width will be used to quantify the benefits of the proposed model.

The steady-state spatial patterns for various receptive field widths ($r > 4$) are shown in Fig. 10. Global connections lead to sparse representation (fewer active mitral cells) since highly active GL regions are able to suppress activity in other regions in the lattice with weak activity. This causes reduction in the overlap across patterns and improves odor separability.

4.3. Temporal evolution of pattern separability

To illustrate the benefits of the proposed model, we compare the resulting pattern-separability against that which is available (1) from raw sensor data, (2) following chemotopic convergence, (3) at the output of the OB network without lateral connections, and (4) at the output of the OB network with random lateral connections. Fig. 11a–c shows the temporal evolution of the separability measures J_{odor}, J_{conc}, and J_{balance} for each of these cases. Fig. 11a indicates that chemotopic convergence provides better concentration-invariant separability than raw temperature-modulated signals. On the other hand, Fig. 11b shows that random connections can in some cases provide better concentration discrimination than center-surround connections, but have significantly lower concentration-invariant separability as shown in Fig. 11a. Overall, center on–off surround lateral connections (three repetitions are shown using different initial weights) provides maximum contrast between odor patterns amongst the compared schemes, and yields maximum value for the joint objective function J_{balance} as shown in Fig. 11c.

5. Summary and conclusions

We have presented a neuromorphic model for processing chemosensor array signals based on two mechanisms in the early

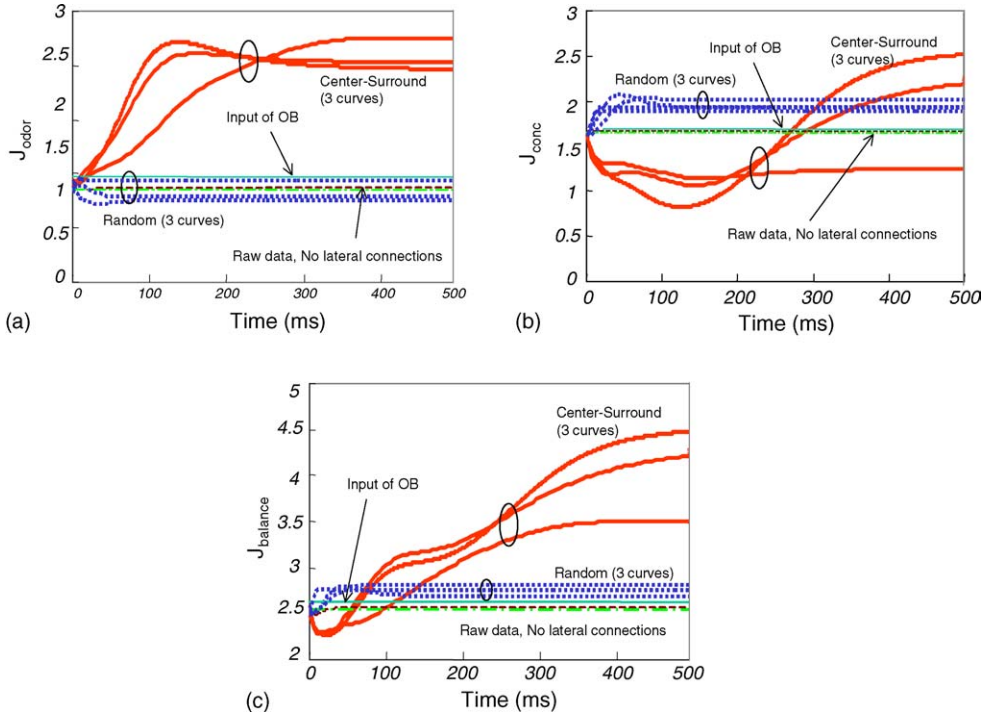

Fig. 11. Comparison of the additive model of OB lateral inhibition with center-surround lateral connections (three repetitions are shown) against (1) raw temperature-modulated data, (2) following chemotopic convergence, (3) at the output of OB with no lateral connections, and (4) at the output of OB with random lateral connections (three repetitions). (a) Concentration-invariant recognition measure J_{odor}, (b) concentration discrimination measure J_{conc}, and (c) balanced measure J_{balance}.

olfactory pathway: chemotopic convergence of ORNs onto GL, and center-surround lateral inhibitory in the olfactory bulb. First, a large population of pseudo-sensors is obtained by modulating the operating temperature of a metal-oxide sensor array. The distribution of pseudo-sensors in chemical affinity space is then captured with a Kohonen SOM. As a result, sensors become clustered according to their selectivity, and a spatial pattern emerges across the lattice.

Following recent results from neurobiology, we model OB lateral inhibitory circuits using a recurrent network with center on–off surround receptive fields. This network is able to significantly reduce the overlap between the odor spatial patterns, and produce a sparser representation on a few selected mitral cells.

To quantify the benefits of the model, we have proposed a novel statistical separability measure that provides the necessary tradeoff between concentration-invariant recognition and concentration sensitivity. We have used this pattern separability measure to characterize the parameters and evaluate the performance of OB network with center on–off surround lateral connections. Our results clearly show that the proposed model consistently enhances contrast and provides better separability between odor patterns.

Acknowledgements

This material is based upon work supported by the National Science Foundation under CAREER award 9984426/0229598. T. Yamanaka is supported by a postdoctoral fellowship for research abroad (2004) from the Japan Society of the Promotion of Science.

References

[1] R. Gutierrez-Osuna, Pattern analysis for machine olfaction: a review, IEEE Sens. J. 2 (3) (2002) 189–202.
[2] M. Pardo, G. Sberveglieri, Learning from data: a tutorial with emphasis on modern pattern recognition methods, IEEE Sens. J. 2 (3) (2002) 203–217.
[3] E.L. Hines, P. Boilot, J.W. Gardner, M.A. Gongora, Pattern analysis for electronic noses, in: T.C. Pearce, S.S. Schiffman, H.T. Nagle, J.W. Gardner (Eds.), Handbook of Machine Olfaction: Electronic Nose Technology, Wiley-VCH, 2003.
[4] J.L. Davis, H. Eichenbaum (Eds.), Olfaction: A Model System for Computational Neuroscience, MIT Press, 1991.
[5] T.C. Pearce, Computational parallels between the biological olfactory pathway and its analogue 'The Electronic Nose'. Part I. Sensor-based machine olfaction, BioSystems 41 (1997) 43–67.
[6] T.C. Pearce, Computational parallels between the biological olfactory pathway and its analogue 'The Electronic Nose'. Part II. Sensor-based machine olfaction, BioSystems 41 (1997) 69–90.
[7] L. Ratton, T. Kunt, T. McAvoy, T. Fuja, R. Cavicchi, S. Semancik, A comparative study of signal processing techniques for clustering microsensor data (a first step towards an artificial nose), Sens. Actuators B41 (1–3) (1997) 105–120.
[8] J. Ambros-Ingerson, R. Granger, G. Lynch, Simulation of paleocortex performs hierarchical clustering, Science 247 (1990) 1344–1348.
[9] J. White, T.A. Dickinson, D.R. Walt, J.S. Kauer, An olfactory neural network for vapor recognition in an artificial nose, Biol. Cybern. 78 (1998) 245–251.
[10] J. White, J.S. Kauer, Odor recognition in an artificial nose by spatio-temporal processing using an olfactory neuronal network, Neurocomputing 26–27 (1999) 919–924.
[11] T.C. Pearce, P.F.M.J. Verschure, J. White, J.S. Kauer, Robust stimulus encoding in olfactory processing: hyperacuity and efficient signal transmission, in: S. Wermter, J. Austin, D. Willshaw (Eds.), Emergent Neural Computation Architectures Based on Neuroscience, Springer-Verlag, 2001, pp. 461–479.
[12] M. Otto, S. Quarder, U. ClauBnitzer, J. Lerchner, A nonlinear dynamic system for recognizing chemicals based on chemical sensors and optical spectra, in: Proceedings of the World Multiconference on Systemics, Cybernetics and Informatics (SCI-2000), vol. X, 2000, pp. 413–418.
[13] H.J. Chang, W.J. Freeman, B.C. Burke, Biologically modeled noise stabilizing neurodynamics for pattern recognition, Int. J. Bifurcation Chaos 8 (2) (1998) 321–345.
[14] R. Gutierrez-Osuna, A. Gutierrez-Galvez, Habituation in the KIII olfactory model with chemical sensor arrays, IEEE Trans. Neural Networks 16 (2003) 649–656.
[15] R. Gutierrez-Osuna, N.U. Powar, Odor mixtures and chemosensory adaptation in gas sensor arrays, Int. J. Artif. Intell. Tools 12 (1) (2003) 1–16.
[16] R. Gutierrez-Osuna, B. Raman, Cancellation of chemical backgrounds with generalized Fischer's linear discriminants, in: Proceedings of Third IEEE Sensors conference, Vienna, Austria, 2004.
[17] B. Raman, R. Gutierrez-Osuna, Concentration normalization with a model of gain control in the olfactory bulb, in: Proceedings of the 11th International Symposium on Olfaction and the Electronic Nose (ISOEN 2005), Barcelona, Spain, April 13–15, 2005, in press.
[18] B. Raman, R. Gutierrez-Osuna, Mixture segmentation and background suppression in chemosensor arrays with a model of olfactory bulb–cortex interaction, in: 2005 IEEE International Joint Conference on Neural Networks, Montreal, Canada, July 31–August 4, 2005, pp. 131–136.
[19] B. Raman, R. Gutierrez-Osuna, Chemosensory processing in a spiking model of the olfactory bulb: chemotopic convergence and center surround inhibition, in: NIPS 2004, Vancouver, BC, December 13–16, 2004.
[20] B. Raman, R. Gutierrez-Osuna, A. Gutierrez-Galvez, A. Perera-Lluna, Sensor-based machine olfaction with a neurodynamics model of the olfactory bulb, in: Proceedings of the 2004 IEEE/RSJ International Conference on Intelligent Robots and Systems, Sendai, Japan, September 28–October 2, 2004.
[21] A.P. Lee, B.J. Reedy, Temperature modulation in semiconductor gas sensing, Sens. Actuators B60 (1999) 35–42.
[22] R. Vassar, et al., Topographic organization of sensory projections to the olfactory bulb, Cell 79 (1994) 981–991.
[23] K. Mori, H. Nagao, Y. Yoshihara, The olfactory bulb: coding and processing of odor molecule information, Science 286 (1999) 711–715.
[24] R. Gutierrez-Osuna, A self-organizing model of chemotopic convergence for olfactory coding, in: Proceedings of the Second Joint EMBS-BMES Conference, Houston, TX, 2002, pp. 23–26.
[25] M. Meister, T. Bonhoeffer, Tuning and topography in an odor map on the rat olfactory bulb, J. Neurosci. 21 (4) (2001) 1351–1360.
[26] B.A. Johnson, M. Leon, Modular representation of odorants in the glomerular layer of the rat olfactory bulb and the effects of stimulus concentration, J. Comp. Neurol. 422 (2000) 496–509.
[27] T. Kohonen, Self-organized formation of topologically correct feature maps, Biol. Cybern. 43 (1982) 59–69.
[28] J. Laaksonen, M. Koskela, E. Oja, Probability interpretation of distributions on SOM surfaces, in: Proceedings of Workshop on Self-Organizing Maps (WSOM'03), Hibikino, Kitakyushu, Japan, 2003, pp. 77–82.
[29] W. Freeman, Olfactory system: odorant detection and classification, in: D. Amit, G. Parisi (Eds.), Building Blocks for Intelligent Systems: Brain Components as Elements of Intelligent Function, vol. III, part 2, Academic Press, New York, 1999.
[30] G. Laurent, A systems perspective on early olfactory coding, Science 286 (22) (1999) 723–728.
[31] J.L. Aungst, P.M. Heyward, A.C. Puche, S.V. Karnup, A. Hayar, G. Szabo, M.T. Shipley, Center-surround inhibition among olfactory bulb glomeruli, Nature 26 (2003) 623–629.

[32] S.W. Kuffler, Discharge patterns and functional organization of mammalian retina, J. Neurophysiol 16 (1953) 37–68.
[33] S. Haykin, Neural Networks: A Comprehensive Foundation, second ed., Prentice-Hall, Englewood Cliffs, NJ, 1999, p. 676.
[34] Figaro 1996. Figaro Engineering, Inc., Osaka, Japan.
[35] R.W. Friedrich, S.I. Korsching, Combinatorial and chemotopic odorant coding in the zebrafish olfactory bulb visualized by optical imaging, Neuron 18 (1997) 737–752.
[36] K. Fukunaga, Introduction to Statistical Pattern Recognition, second ed., Academic Press, New York, 1990.

Biographies

Baranidharan Raman received the Bachelor of Engineering in Computer Science with distinction from the University of Madras in 2000, and the M.S. and Ph.D. degrees in Computer Science from Texas A&M University in 2003 and 2005, respectively. His research interests include sensor based machine olfaction, intelligent systems, machine learning, neural computation, and robotics.

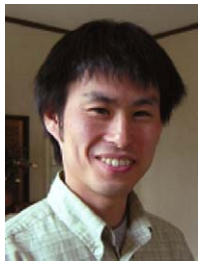

Takao Yamanaka received the Bachelor of Engineering, the Master of Engineering, and the Ph.D. in Engineering from Tokyo Institute of Technology in 1996, 1998, and 2004, respectively. He was with Canon, Inc. from 1998 to 2000 in the area of image and signal processing. He is currently a postdoctoral fellow at Texas A&M University, supported by JSPS postdoctoral fellowship for research abroad. His research interests include neuromorphic engineering, intelligent sensors, machine learning, computational neuroscience, and machine olfaction.

Ricardo Gutierrez-Osuna received the B.S. degree in Electrical Engineering from the Polytechnic University of Madrid in 1992, and the M.S. and Ph.D. degrees in Computer Engineering from North Carolina State University in 1995 and 1998, respectively. From 1998 to 2002 he served on the faculty at Wright State University. He is currently an assistant professor of Computer Engineering at Texas A&M University. His research interests include pattern recognition, neuromorphic computation, machine olfaction and speech-driven facial animation.